High-Rate Mechanical Properties of Human Heel Pad for Simulation of a Blast Loading Condition

Lee F. Gabler, Matthew B. Panzer, Robert S. Salzar

Abstract Lower extremity injuries are a major concern for military personnel exposed to blast loading in armored vehicles. The primary mechanism of injury during these events has been identified as high-rate axial loading to the heel through local deformation of the vehicle floor. Hence, heel mechanics play an important role in the load path and overall lower limb response during high-rate loading events. In this study, rate-dependent mechanical properties for the human sub-calcaneal heel pad were determined using a quasi-linear viscoelastic constitutive model. Tissue samples were characterized up to 45% compression at peak strain rates of $57s^{-1}$, using a ramp and hold test protocol. The results were incorporated into a finite element (FE) model of the lower limb previously developed and validated for automotive impact applications. The modified FE model with updated heel properties demonstrated superior biofidelity over the original model when compared to experimental impact tests performed at blast loading rates on cadaveric specimens; correlation and analysis scores increased by 0.37, on average, for force time-history response. This work constitutes preliminary steps required for the development of an effective and biofidelic modeling tool that may be used for evaluating future systems designed to mitigate injury in underbody blast events.

Keywords Constitutive modeling, Finite element modeling, Heel pad, Lower extremity injury, Underbody blast

I. INTRODUCTION

Reports of severe lower extremity injuries from the battlefield highlight a serious problem for soldiers exposed to blast loading in armored vehicles [1]. These injuries include foot, ankle and lower limb fractures and account for more than 80% of all skeletal injuries observed in survivors of underbody blast (UBB) events [2]. The most recent battlefield epidemiology suggests that these injuries are caused by high-rate axial loading to the lower extremities from contact forces between the deforming vehicle floor and the occupant's feet [2]. Further, vehicle floor deformations have been reported to reach 30m/s in 6ms suggesting that floor acceleration in armored vehicles during a UBB event may exceed 500g in 2-3ms [2-3].

A major concern in automotive safety is the large number of severe injuries to the foot and ankle caused by axial loading to the lower limb which has been associated with an intruding foot-pan during frontal vehicular crashes [4]. Research on foot and ankle injury mechanisms for these impacts has led to a well-established body of knowledge for injury risk and preventative strategies including the development of anthropometric test devices (ATDs) and computational models. One such contribution that can be leveraged from the automotive field is the use of advanced, injury-predictive finite element (FE) models of the lower extremity [5-6]. FE models are well-suited to help study and predict the high-rate dynamics of the lower extremities caused by automotive type impacts, and have the potential for investigating biomechanical response in UBB events. Further, these models offer a means of reproducing the effects of blast type loading on the lower extremity in a cost effective manner.

One of the limitations associated with current automotive ATDs and FE models is their lack of predictive capability for high-rate loading applications. For example, load rate dependent material properties for the sub-calcaneal heel pad have not been incorporated into FE models, while the rubber material used in the feet of ATDs are effectively much stiffer than those of the fleshy tissue they represent [7-9]. In the event of high-rate axial loading to the lower extremity, the soft tissue layer in the plantar region of the foot is typically the first structure engaged. Consequently, the material properties of this structure may have a strong influence on the

L.F. Gabler is a Ph.D. candidate (phone: +1 434 296 7288, email: lfg4dc@virginia.edu), M.B. Panzer, Ph.D. is an associate professor, and R.S. Salzar, Ph.D. is the principal scientist in Department of Mechanical and Aerospace Engineering at the University of Virginia's Center for Applied Biomechanics, Charlottesville, VA, USA.

overall mechanical response of the lower limb during blast loading. Hence, accurate heel compression characteristics, which incorporate rate-sensitivity, must be included to help improve ATDs and FE models of the lower limb for applications in blast-type loading events such as UBB. In this study, rate-sensitive mechanical properties for the human sub-calcaneal heel pad were characterized under high-rate, uniaxial compression through a constitutive framework commonly used to model various other soft biological materials. The determined properties were then implemented into the current automotive FE model to improve fidelity for high-rate loading applications. Fidelity of the updated heel pad properties as well as the improved model was evaluated using previously acquired experimental high-rate impact data on cadaveric lower limbs [10].

II. METHODS

Materials

Protocols for the handling of biological materials were approved by the University of Virginia's Institutional Biosafety Committee. Five whole heel pads were collected from the hind foot region of three post mortem human surrogates (PMHS), Table 1. PMHS specimens were prescreened for Hepatitis A, B, and C in addition to HIV, and were cryogenically frozen within 48 hours of death to prevent decomposition of the tissue. Following collection, the heel pads were refrozen and stored in a morgue freezer at -20°C until materials testing could be performed. Materials testing occurred over the course of several days, and approximately two months following heel pad collection. On the day of a particular test one to two whole heel pads were partially thawed at room temperature for 30min to make sample cutting easier. Several cubic samples were cut from each whole pad and consisted of various substructures including the skin, both small and large adipose chambers, and connective septa. Incisions were made perpendicular to the surface of the skin, by hand, using a scalpel. Digital calipers and a T-square were used to mark square dimensions on the plantar surface of the pad to help guide the incisions. The number of samples collected from a single pad was determined by the size of the tissue; less samples were taken from smaller heel pads which tended to thaw quicker making it difficult to cut samples with uniform dimensions. If a pad completely thawed, it was discarded and not re-frozen for later use. This was done in order to prevent inclusion of samples with further damage to the material due to multiple freeze-thaw cycles. The height of each sample was trimmed by carefully removing a thin layer of dorsal adipose tissue using the scalpel. Samples with different heights were created to vary the range of strains and strain rates that could be applied to the tissue. Each sample was qualitatively assessed prior to testing, and those that were highly distorted were discarded; seventeen out of the twenty total excised samples were used for materials testing. The height and two arbitrarily chosen orthogonal sides were measured using digital calipers. The dimensions were, on average, (12.90±2.37)mm for the height and (15.37±2.01)mm for both sides combined. Since the samples were not perfectly square, the percentage difference between the two orthogonal sides on a particular sample was, on average, (11±11)%.

TABLE 1
PMHS INFORMATION

Specimen #	Gender	Age (yr)	Stature (cm)	Weight (kg)	Heel Pad ID	# of Samples
534	M	71	173	95.2	534R	3
					534L	1
641	M	55	170	102.1	641R	5
					641L	6
653	M	52	175	72.1	653L	2

Mechanical Testing

Heel pad samples were tested under uniaxial compression using a bench-top test machine (ElectroForce® 3100, Bose Corporation – ElectroForce, Eden Prairie, MN). Samples were placed on an aluminum stage mounted atop a fixed 5lb capacity force transducer (Model 31 Low, Honeywell International Inc., Golden Valley, MN) and beneath a flat aluminum load platen mounted to a linear actuator equipped with an LVDT to measure displacement. The tissue was oriented such that the adipose layer was contacting the load platen and a thin layer of saline was applied to both the top and bottom platens to ensure a stress-free boundary condition during compression. Prior to testing, a 50mN pre-compressive force was applied to the tissue by carefully adjusting the actuator. This provided an even loading condition across the surface of the sample. The distance between platens was then measured and taken as the initial, un-deformed sample height. In most tests this height was within 1mm of the original height. The top platen was then rapidly pressed into the tissue and held for 30s to measure the relaxation. Samples were compressed up to (10-45)% engineering strain at different effective strain rates; the smallest on average was $0.001 s^{-1}$ and the highest on average was $30 s^{-1}$, with a peak of $57 s^{-1}$ (Table 2). Four tests were performed with constant strain rates less than or equal to $1 s^{-1}$. The peak strain rates achieved in the other thirteen tests were between $(10\text{-}57) s^{-1}$. Due to physical limitations of the actuator, tests performed at strain rates of $10 s^{-1}$ or higher could not be applied at a constant rate. Five minutes were allotted in between pre-compression and testing to ensure full recovery of the tissue. All samples were tested only once.

TABLE 2
MECHANICAL TESTING MATRIX

# of Samples	Strain (%)	Peak Strain Rate (s^{-1})
3	10	13
3	20-24	10-27
6	25-30	0.01-50
5	40-45	0.001-57

Data Analysis and Constitutive Modeling

Force and displacement data were acquired at 20kHz for all mechanical tests (DEWE-2010, Dewetron Inc., Wakefield, RI). Raw data were filtered using a zero-phase shift, digital 8 pole IIR Butterworth filter at a low pass frequency of 400Hz. Logarithmic resampling was applied to give equal weighting to both the ramp and hold portions of the test for the purpose of fitting the data. Once processed, engineering stress, σ, and engineering strain, ε, were calculated from the force displacement data. The stress response, $\sigma(\varepsilon, t)$, to an arbitrary strain input, $\varepsilon = \varepsilon(t)$, was modeled using a quasi-linear viscoelastic (QLV) mathematical framework [11]:

$$\sigma(\varepsilon, t) = \int_0^t G(t - t') \frac{\partial \sigma^e(\varepsilon)}{\partial \varepsilon} \frac{\partial \varepsilon}{\partial t'} dt' \quad (1)$$

where $\sigma^e(\varepsilon)$ is the instantaneous elastic response (IER) and $G(t)$ is the normalized or reduced relaxation function (RRF), $0 \le G(t) \le 1$. The elastic behavior of the tissue was modeled using an exponential function:

$$\sigma^e(\varepsilon) = A[e^{B\varepsilon} - 1] \quad (2)$$

where A and B are constants, note $\sigma^e(0) = 0$. Exponential models are commonly used to model soft biological materials [11-13]. A prony series with five time constants was chosen to model the relaxation behavior:

$$G(t) = G_\infty + \sum_{i=1}^{5} G_i \cdot e^{-\frac{t}{\tau_i}} \quad (3)$$

where G_i's are the normalized relaxation coefficients of the corresponding time decades and G_∞ is the coefficient of the approximated steady-state response, $G_\infty = 1 - \sum G_i$. An F-Test revealed that five time constants were sufficient to model the data and that there was no significant improvement in fit with the addition of a sixth time constant ($p > 0.05$). Further, five time constants had a significant improvement in fit over four ($p < 0.05$). Values for the coefficients A, B, τ_i, and G_i were determined through a reduced gradient algorithm (Excel Solver®, Microsoft®, Redmond, WA) that was used to minimize the sum squared error (SSE) between the experimental data and model-predicted force. Initial fitting of the model to the experimental data resulted in marginal variability in the values for the optimized time constants, τ_1≈0.001s, τ_2≈0.01s, τ_3≈0.1s, τ_4≈1s, and τ_5≈10s. To simplify the model and improve stability of the fitting algorithm, the time constants were fixed at these decades for the remainder of the analysis and only the parameters of $\sigma^e(\varepsilon)$ and $G_i$were determined.

To overcome the challenges associated with developing a predictive model for data with vast differences in the level of applied strain and strain rates, the following fitting procedures were employed: All seventeen datasets were fit individually and an optimal set of coefficients for the functions of $\sigma^e(\varepsilon)$ and $G(t)$ were determined for each test. This procedure resulted in large variability in $\sigma^e(\varepsilon)$ (defined as model 1.1), while $G(t)$ was more consistent across the fits. To improve the viability of the model, an average $G(t)$ was calculated and then used to refit each dataset. This procedure resulted in less variability in $\sigma^e(\varepsilon)$ (defined as model 1.2), across all datasets improving the overall predictive power of the model. A characteristic $\sigma^e(\varepsilon)$ (defined as model 1.3) was then determined by minimizing the SSE between the individual fits and the characteristic curve. All data were fit over the entire duration of the time-history.

Finite Element Modeling

Fidelity of the lower limb FE model was evaluated using the Phase I lower extremity of the Global Human Body Model Consortium (GHBMC) 50th percentile male (version 3.5) in a configuration representative of an UBB loading environment (Figures 1 and 2). The foot-ankle-leg model was previously developed and validated for a wide range of loading conditions stemming from automotive-type impacts [5-6]. This model was integrated into a separate FE model in a configuration similar to experimentally reported drop-tower tests on PMHS lower limbs (Figure 2) [10]. In that study, each leg was sectioned above the proximal epiphysis of the tibia and fibula, and instrumented with accelerometers, strain gauges and load cells. The lower limbs were mounted at the bottom of a drop-tower equipped with an impactor capable of producing axial loading on the foot up to 600 g's of acceleration over a (2-3)ms duration. The FE model was used to simulate impacts from eleven of the eighteen lower limbs tested in that study. Experimental acceleration time histories from those tests were prescribed to the impact plate. The model included a preload of 100N corresponding to the impact plate resting on top of the foot prior to impact in the experiment. A free plate attached to the potted end of the tibia via a load cell element was included in the model and weighed 6.2kg. This mass was chosen to represent the recruited mass of the thigh during high-rate loading [10]. Comparison between the FE model and physical data was made by focusing on the corresponding load cell force and strain measured at the proximal and distal tibia, respectively. Each simulation was run for 15ms using commercial FE software (LS-DYNA V971 R6.1.1., LSTC, Livermore, CA).

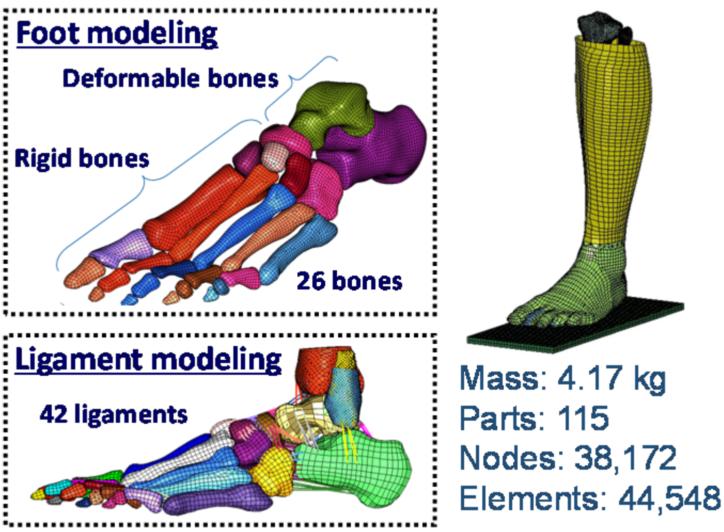

Fig. 1. Lower limb FE model for the GHBMC developed at the University of Virginia. The model is representative of a 50% percentile male (175cm stature, 77kg body weight)

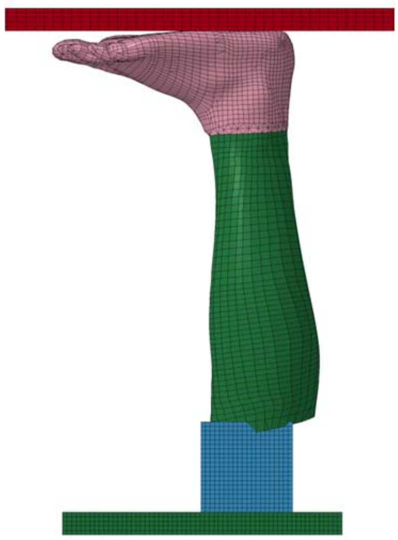

Fig. 2. FE model in a configuration representing the experimental test setup of Henderson et al. [10].

An initial series of simulations were performed using the original version of lower limb FE model to establish a baseline for comparison with the experimental results. Following that analysis, the model was modified to better reflect the experimental data. Three modifications were considered: First, the constitutive properties for the heel pad, developed in the current study, were incorporated into the foot flesh of the GHBMC. This update was added to improve the dynamic, viscoelastic characteristics of the foot which were not previously incorporated into the original FE model. Second, the meshes for several bones were refined to produce a more accurate geometry in the ankle joint, and to increase the number of through-thickness elements in the fibula and tibia shafts from one to two (Figure 3). Computed tomography images were used to improve both topology and mesh quality over the original model. Third, the material properties of the cortical and cancellous bone in the tibia and fibula were updated with more recent properties available in the literature [14-17]. Detailed specifications for each modification are listed in Tables 3 and 4.

Simulations were rerun with the same boundary conditions as the original model and the resulting forces and strains were compared. To determine the contribution of each modification on the overall response, a parametric analysis was performed on the FE model using the experimental data from test 1.13 of Henderson et al. [10]. Model accuracy to the experimental data was assessed using the cross-correlation methods of correlation and analysis (CORA) [18]. Phase, size and shape parameters were given equal weighting to form the overall CORA score. A general linear model (GLM) was used to evaluate the contribution of each modification on the overall improvement in response of the FE model. Coefficients of the GLM indicate the change in each CORA cross-correlation score for a particular model modification. Student's t-test was used to evaluate whether or not a particular GLM coefficient was significant, $\alpha=0.05$.

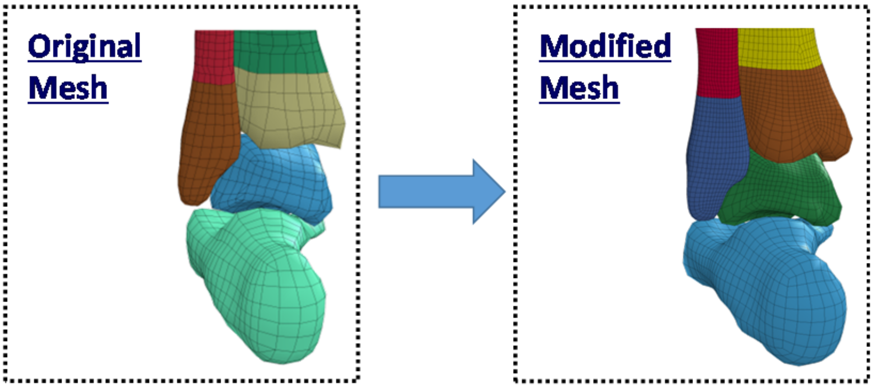

Fig. 3. Mesh modifications made to the GHBMC FE model. Element size was decreased for several bony structures including the tibia, fibula, calcaneus and talus. Re-meshing characteristics are listed in Table 3.

TABLE 3
RE-MESHING CHARACTERISTICS

Bone	Original Mesh Size (mm)	Modified Mesh Size (mm)
Tibia	3.8	1.9
Fibula	2.2	1.1
Calcaneus	4.7	3.2
Talus	4.1	2.3

TABLE 4
MATERIAL RE-MODELING

Structure	Original Model	Modified Model
FOOT-FLESH (Heel Pad)	*MAT_OGDEN_RUBBER (ρ=1g/cm^3, ν = 0.49)	*MAT_SIMPLIFIED_RUBBER/FOAM (K = 2GPa)
Tibia/Fibula (Cortical)	*MAT_STRAIN_RATE_DEPENDENT_PLASTICITY (ρ=2g/cm^2, E=17.5GPa, σ_Y=125MPa, ν=0.3)	*MAT_PIECEWISE_LINEAR_PLASTICITY (σ_Y=140MPa, σ_U=214, ε_U=2.2%)
Tibia/Fibula (Cancellous)	*MAT_PLASTIC_KINEMATIC (ρ=1.1g/cm^2, E=455MPa, σ_Y=5.3MPa, ν=0.3)	*MAT_PIECEWISE_LINEAR_PLASTICITY (E=1.07GPa, σ_Y=8.56MPa, ν=0.1, σ_U=8.564, ε_U=13.4%)
Talus (Cortical)	*MAT_PLASTIC_KINEMATIC (ρ=2g/cm^2, E=17.5GPa, σ_Y=165MPa, ν=0.29)	*MAT_PIECEWISE_LINEAR_PLASTICITY (σ_Y=140MPa, ν=0.3, σ_U=214, ε_U=2.2%)
Talus (Cancellous)	*MAT_PLASTIC_KINEMATIC (ρ=1.1g/cm^2, E=455MPa, σ_Y=5.3MPa, ν=0.3)	*MAT_PIECEWISE_LINEAR_PLASTICITY (E=1.070GPa, σ_Y=8.56MPa, ν=0.1, σ_U=8.564, ε_U=13.4%)
Calcaneus (Cortical)	*MAT_PLASTIC_KINEMATIC	*MAT_PIECEWISE_LINEAR_PLASTICITY

	(ρ=2g/cm^2, E=17.5GPa, σ_Y=165MPa, ν=0.29, σ_U=178MPa, ε_U=2.2%)	(σ_Y=140MPa, ν=0.3, σ_U=214)
Calcaneus (Cancellous)	*MAT_PLASTIC_KINEMATIC (ρ=1.1g/cm^2, E=455MPa, σ_Y=5.3MPa, ν=0.3)	*MAT_PIECEWISE_LINEAR_PLASTICITY (E=68MPa, σ_Y=544kPa, ν=0.1, σ_U=8.24, ε_U=13.4%)

ρ=Density, ν=Poisson's Ratio, E=Young's Modulus, σ_Y=Yield Stress, K=Bulk Modulus, σ_U=Ultimate Stress, ε_U=Ultimate Strain. Values for material properties not reported in the new model remain unchanged from the original model.

III. RESULTS

The heel pad material exhibited spatial non-linearity and behaved viscoelastically; relaxation was observed in the force time history following the peak force and during the displacement hold. Fitted values for the coefficients of the optimized model (model 1.3) are presented in Table 5. Overall model response fit to the experimental data is provided in Figure 4. Average R^2 for model 1.3 fit to the seventeen experimental datasets was 0.98. Development of the characteristic $\sigma^e(\varepsilon)$ by fitting model 1.3 to the individual fits of model 1.2 is presented in Figure 4, A, while the average $G(t)$ is shown in Figure 4, B. Model characterization of the experimental data suggests a good fit, considering the large variability generated by testing cadaveric material. Using these results and equations (1-3), stress-strain curves for a range of constant strain rate inputs (0.1-10000)s^{-1} were constructed and implemented into the FOOT-FLESH (heel pad) material in the GHBMC FE model (Figure 5). The data generated using the QLV constitutive model were extrapolated out to 90% engineering compressive and tensile strain to ensure mathematical stability of the material during loading in FE simulations. Tensile data were calculated by assuming symmetry of equation (2) about the origin.

(A)

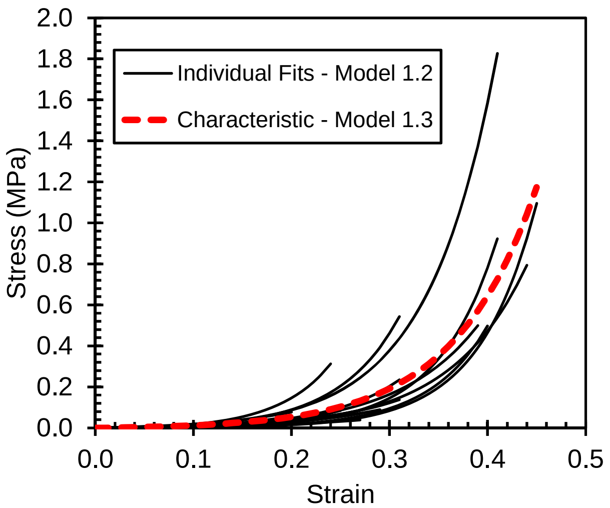

(B)

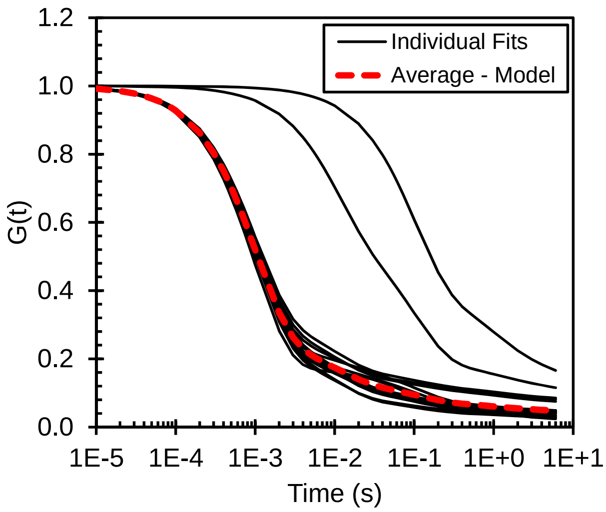

(C)

(D)

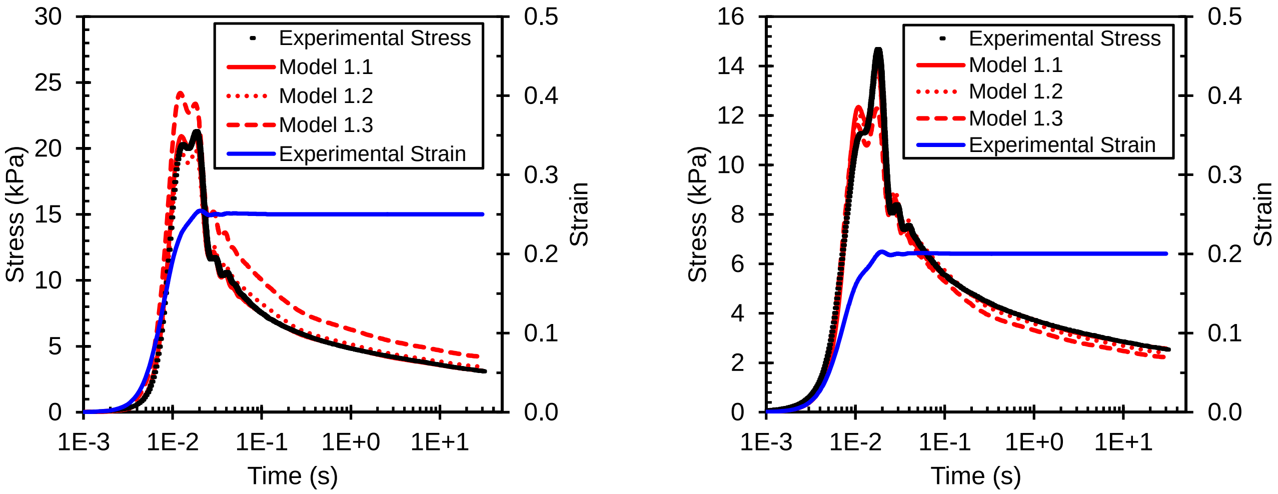

(E)

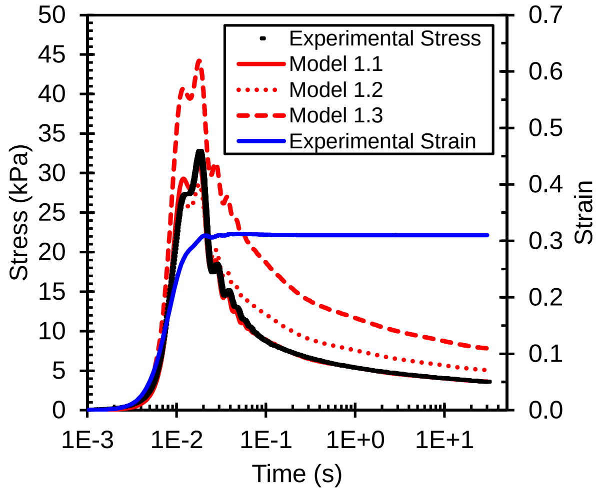

(F)

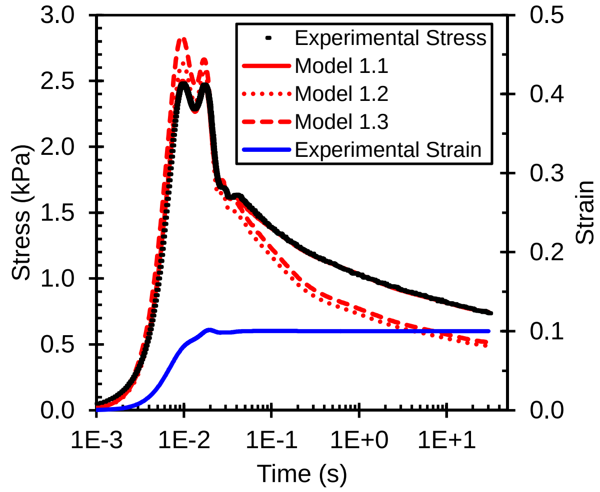

Fig. 4. QLV model fit to the experimental heel pad data. Characteristic curve (model 1.3) for (A) $\sigma^e(\varepsilon)$ and average curve for (B) $G(t)$. In the case of $G(t)$ the average included only individual fits within the main grouping; the two traces outside this grouping were not averaged. (C-F) progression of the model fitting protocol to the experimental data for a selection of representative datasets. Notice that the final model 1.3, predicts the response of data fairly well in cases (C-D). However, the fits in cases (E-F) were not as predictive. This is likely a result of the high variability in the experimental data. All plotted data reflects compressive engineering stresses and strains.

TABLE 5

OPTIMIZED VALUES FOR THE COEFFICIENTS OF $\sigma^e(\varepsilon)$ AND $G(t)$

Units	Coefficients	Fitted Values
kPa	A	5.51
-	B	11.9
-	G_1 (τ_1 = 0.001s)	0.741
-	G_2 (τ_2 = 0.01s)	0.125
-	G_3 (τ_3 = 0.1s)	0.059
-	G_4 (τ_4 = 1s)	0.020
-	G_5 (τ_5 = 10s)	0.015
-	Ginf ($\tau \rightarrow \infty$)	0.040

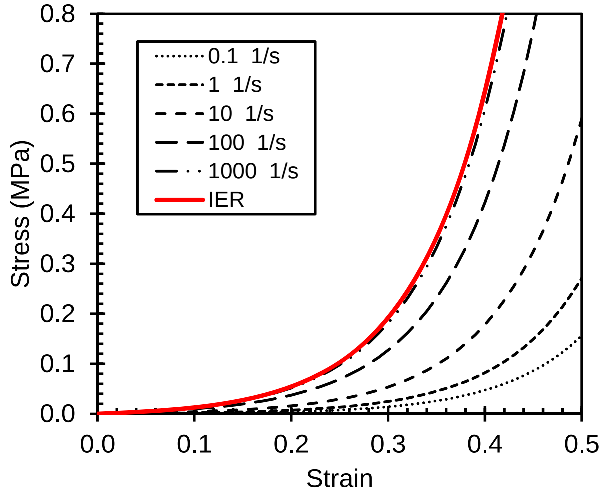

Fig. 5. Load curves generated using eq. (1-3) and model parameters listed in Table 5. Each curve was generated using a constant strain rate input. Six rates were chosen: $0.1s^{-1}$, $1s^{-1}$, $10s^{-1}$, $100s^{-1}$, $1000s^{-1}$, and $10000s^{-1}$. The $10000s^{-1}$ curve was nearly identical to the IER. Since the curves are symmetric about the origin, they represent both tensile and compressive stresses and strains. The load curves were implemented into LS-DYNA (MAT_181) which interpolates stress based on strain and strain rate from a look-up table containing these curves.

Results from the original FE model grossly underestimated both the proximal tibia force and anterior, posterior distal tibia strains when compared to the experimental impact data (Figures 6 and 7). Peak compressive forces and strains generated in the original model were severely attenuated. Further, a significant phase delay was observed between experimental and model time histories during both loading and unloading of the foot. Modifications to the original model greatly improved biofidelity; peak forces were more representative of the values measured experimentally and the phase shift observed in the original model was nearly eliminated (Figure 6). The modified model more accurately predicted loading and unloading of the experimental data; the average overall CORA score increased by 0.37 from (mean±S.D.) (0.53±0.05) to (0.90±0.08). Phase response and magnitude for the anterior and posterior distal tibia strains also greatly improved with modifications to the original FE model; however, the model continued to under-estimate peak strain over all tests (Figure 7). The average improvement in overall CORA score for the anterior and posterior strains was from (0.42±0.09) to (0.70±0.23) and from (0.45±0.13) to (0.59±0.23), respectively. Mean CORA values including scores for the phase, shape and size parameters for original and modified tibia forces and strains are listed in Table 6.

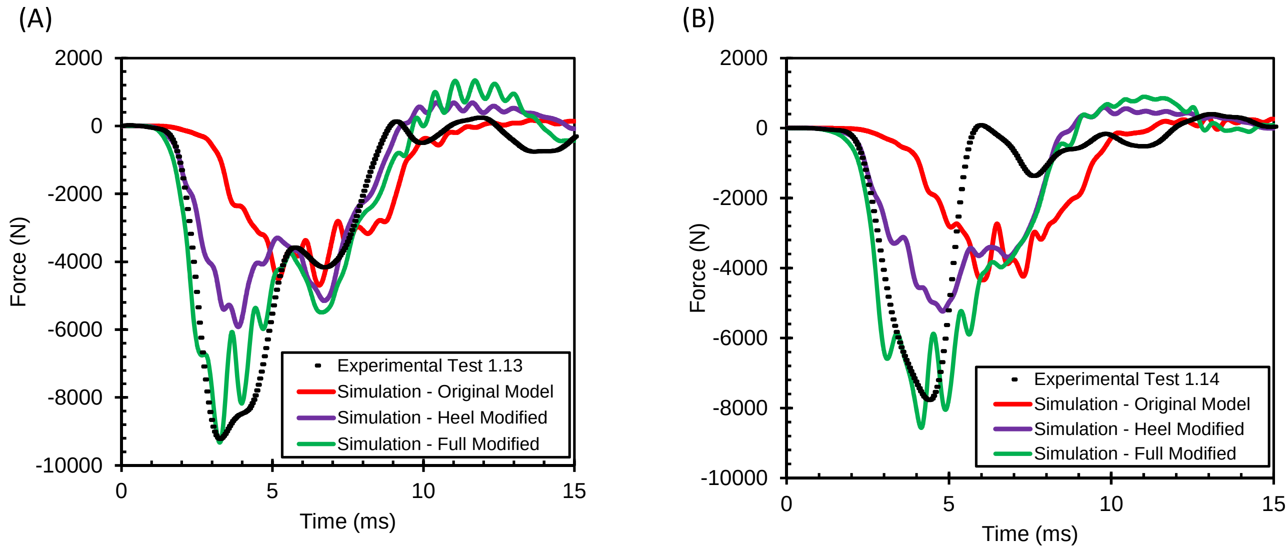

Fig. 6. Comparison of original and modified proximal tibia forces for two representative tests (A) 1.13 and (B) 1.14 from [10]. The model in which only heel constitutive properties were updated (Heel Modified) is included for comparison. Note the improvement in phasing achieved by modifying only the heel properties. The average phase score improvement across all eleven tests was 0.68; (0.30±0.18) to (0.98±0.02).

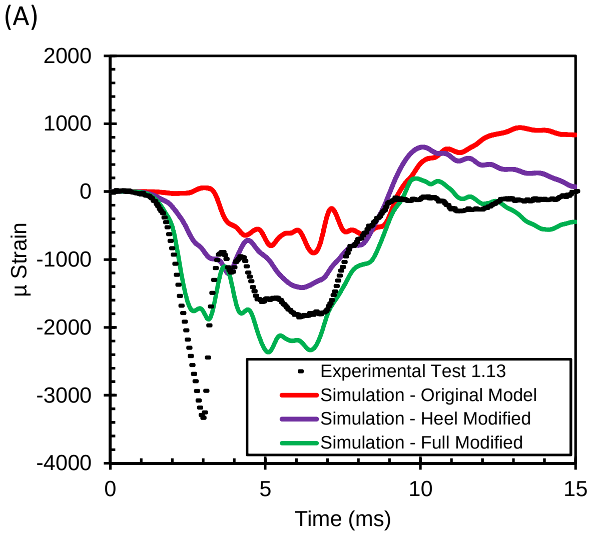

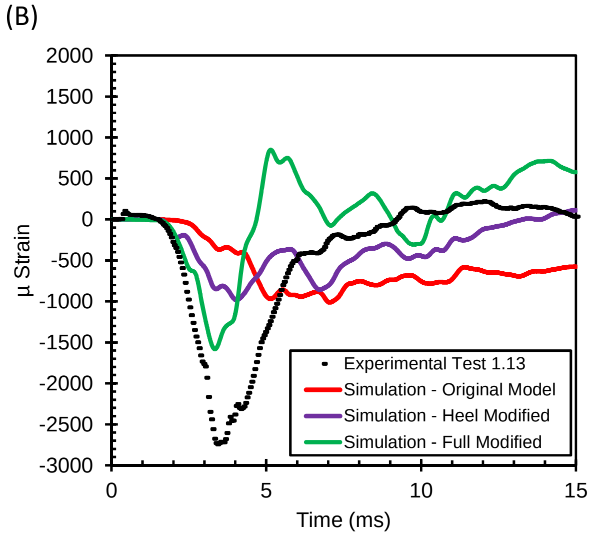

Fig. 7. Comparison of original and modified distal tibia strain time histories for a representative test, 1.13 (A) anterior strain and (B) posterior strain. The average phase score improvement across all eleven tests was 0.38; (0.23±0.26) to (0.61±0.45) for the anterior strain and 0.36; (0.28±0.32) to (0.64±0.42) for the posterior strain.

TABLE 6
MEAN CORA SCORES

	Proximal Tibia Force		Anterior Distal Tibia Strain		Posterior Distal Tibia Strain	
Scoring	Original Model	Full Modified	Original Model	Full Modified	Original Model	Full Modified
Overall	(0.53±0.05)	(0.90±0.08)	(0.42±0.90)	(0.70±0.23)	(0.45±0.13)	(0.59±0.23)
Phase	(0.30±0.18)	(0.98±0.02)	(0.23±0.26)	(0.61±0.45)	(0.28±0.32)	(0.64±0.42)
Size	(0.34±0.12)	(0.74±0.22)	(0.26±0.19)	(0.64±0.24)	(0.26±0.21)	(0.30±0.28)
Shape	(0.96±0.02)	(0.97±0.02)	(0.78±0.08)	(0.86±0.12)	(0.81±0.14)	(0.82±0.13)

Results from the parametric analysis of test 1.13 revealed that updating the heel pad properties and re-meshing bony structures had the greatest contribution to overall model improvement. Modifications involving the heel pad showed a statistically significant improvement in the phasing of the force time-history (0.575, $p < 0.001$), while the improvement in magnitude (shape) was marginally significant (0.336, $p = 0.032$) (Table 7). Phasing for the strain response was also significantly affected by modifying the heel properties (0.504, $p = 0.003$) and (0.680, $p < 0.001$) for the anterior and posterior distal tibia strains, respectively (Tables 8 and 9). Re-meshing modifications improved both force and strain amplitudes, however failed to improve the problems associated with phasing. Modifications to the bone properties did not have a significant effect on overall model improvement. Values for the coefficients of the GLM for each modification are reported in Tables 7-9.

TABLE 7
GENERAL LINEAR MODEL COEFFICIENTS FOR PROXIMAL TIBIA FORCE

Modification	Overall	Phase	Size	Shape
Mesh	0.111*	-0.004	0.333*	0.003
Bone	-0.015	0.013	-0.064	0.006
Heel Pad	0.305*	0.575*	0.336*	0.005
R^2	0.957	0.999	0.858	0.724

*Indicates a statistically significant result ($p < 0.05$)

TABLE 8
GENERAL LINEAR MODEL COEFFICIENTS FOR ANTERIOR DISTAL TIBIA STRAIN

Modification	Overall	Phase	Size	Shape

Mesh	0.145*	-0.031	0.280	0.186*
Bone	-0.036	0.022	-0.071	-0.059
Heel Pad	0.299*	0.504*	0.300	0.092
R^2	0.923	0.909	0.779	0.829

*Indicates a statistically significant result ($p < 0.05$)

TABLE 9
GENERAL LINEAR MODEL COEFFICIENTS FOR POSTERIOR DISTAL TIBIA STRAIN

Modification	Overall	Phase	Size	Shape
Mesh	0.023	0.092	-0.077	0.054
Bone	0.019	0.057	0.048	-0.047
Heel Pad	0.183*	0.680*	-0.111	-0.018
R^2	0.938	0.961	0.494	0.468

*Indicates a statistically significant result ($p < 0.05$)

IV. DISCUSSION

Constitutive Modeling of Heel Pad

A number of studies have investigated the compressive characteristics of the human sub-calcaneal heel pad and have used various in vivo and in vitro approaches to characterize the tissue. Although the constitutive models developed in many of these studies incorporate rate-sensitivity and spatial nonlinearity, the applied load rates are still within the range of normal physiological loading and likely well below those experienced in blast. Gefen et al. (2001) measured heel deformation during heel to ground contact through walking [19]. They measured a maximum heel pad compression of 30% with an effective strain of $2.5s^{-1}$. Others have used an in vitro approach to characterize heel pad at much higher rates. Ledoux et al. (2004) and (2007) investigated the viscoelastic behavior of plantar soft tissues including the tissue beneath the heel and metatarsals [12-13]. They observed regional variability in the material properties across the bottom of the foot. Strain rates achieved in those studies were no greater than $10s^{-1}$, typical of low speed automotive type intrusion loading [20].

The highest loading rates previously reported for heel pad were achieved by Miller-Young et al. [21]. In that study, mechanical tests were performed up to 50% compression at constant strain rates varying from $(0.0001\text{-}42)s^{-1}$. Natali et al. fit these data using a hyper-viscoelastic constitutive model and reported viscous parameters for the heel pad [8]. However, the time constants used to fit the data in that study were not representative of the loading rates testing experimentally and would likely lead to inaccuracies if used at higher rates. Although the average, effective strain rates achieved in the current study are within the values reported in the literature, the peak strain rates achieved in three of the seventeen tests were higher, $(50\text{-}57)s^{-1}$. Further, a conservative methodology was used to fit the experimental data in which the time constants were fixed at decades corresponding to the time scales associated with the ramp and hold tests.

In the current study, the mechanical response of the heel pad was found to be stiffer, by nearly one order of magnitude, than results reported previously [8], [12-13], [21]. These discrepancies are likely due to differences in testing methods. In the current study, the mechanical response of cubic heel pad samples, which incorporated skin layers, was characterized in order to develop an effective model for heel pad compression. The samples tested by Miller-Young et al. were of cylindrical shape and trimmed on both the dorsal and plantar surfaces. In trimming the plantar surface they removed the skin layers which may have resulted in a significantly softer response compared to the current study. In general, in vitro testing involves cutting the tissue which disrupts material continuity and may potentially result in forces that are considerably different than those seen in vivo.

There are a number of limitations associated with the current constitutive model developed for the heel pad. The QLV model represents an effective response of the material; traditional engineering material properties were not determined. Previous studies that have developed constitutive models for heel pad assume isotropy and incompressibility allowing for the calculation of material constants [7-9], [21]. Although the assumption of incompressibility is reasonable, the assumption of the deformation gradient may not be. Various layers of skin, adipose and connective tissue make the heel pad structure complex and highly heterogeneous. Despite our best efforts, uniform, unconfined expansion of the material over the entire height was not achieved experimentally. Therefore, a one dimensional, effective mechanical response was characterized in current study. Further, eleven out of the seventeen samples used for mechanical testing were taken from a single PMHS (Table 1). Testing samples from different PMHS would result in mechanical properties more representative of the population.

The tensile constitutive relationship was approximated using symmetry of the instantaneous elastic response about the origin. The instantaneous elastic response was developed under compressive loading and may grossly underestimate the response of the material in tension. Although the event of interest is mainly compressive, tensile stresses are generated through loading of the complex foot geometry. Further, caution should be exercised when using the load curves for the heel pad beyond the strain levels used to characterize the tissue experimentally. Tissue compression up to 90% would result in extreme non-linearity due to compactness of the material and dramatic changes in the tissue geometry. It is likely that a 90% compression predicted by the model severely underestimates the true stress-strain relationship for the heel pad.

Finally, the strain rates tested in the current study are likely much lower than those experienced during blast-type loading. Using the FE model of the lower limb, an effective strain rate for the heel pad was calculated to be $250s^{-1}$, more than four times the peak rates achieved in mechanical testing. This estimation is the current best approximation for the effective strain rates achieved during high-rate axial loading to the heel. However, it is encouraging that after modifying the heel pad with higher rate properties than what is currently available in the literature, a significant improvement in model predictive capabilities was observed.

Finite Element Modeling using GHBMC

Comparison of the original and modified FE model response using experimental impact tests on cadaveric lower limbs indicated significant improvement in the high-rate compression characteristics of heel pad. The original properties for the heel pad in the GHBMC model were taken from Erdemir et al. (2009) [7]. In that study, the heels of 40 volunteers were indented quasi-statically up to 50% compression at a constant strain rate of $0.62s^{-1}$, well below the rates associated with walking and impact traumas. They characterized the data using a hyper-elastic Ogden model without including rate sensitivity. Failure to incorporate tissue viscoelasticity into the model severely limited the utility of their results for high-rate loading applications. Therefore, it is suggested that the constitutive model developed for heel pad in the current study be used for more accurate prediction of lower limb response during high-rate axial loading to the heel.

While great strides were made to convert an FE model of the lower extremity for automotive impacts into a biofidelic model for high-rate military impacts, the effort is ongoing. Many areas of the model have been identified as potential components for further improvement in model biofidelity. First, the constitutive models for bone must account for the high strain rate regimes achieved in military-type impacts. Early work on human bone mechanical properties by McElhaney and Carter and Hayes revealed that the elastic response as well as the yield and ultimate strength of bone were sensitive to loading rate, viscoelasticity and viscoplasticity, respectively, while both of these characteristics were found to be dependent on bone density [22-23]. Many of the constitutive models used for modeling bone were developed based on the elastic-plastic response of metals; they often included viscoelastic or viscoplastic material response but never both. Incorporating more appropriate constitutive models for bone may improve biofidelity of the model in the areas of stress wave propagation and dissipation along the tibia.

Additionally, variations in the ankle's bone properties can strongly affect the fracture response and load transmission through the leg. The strength and stiffness of cancellous bone in the calcaneus, talus and tibia exhibit strong regional dependency [24-25]. Variations in bone strength undoubtedly affect the fracture pattern and tolerance of the bone, which will affect the timing and magnitude of the peak force sustained in the lower limb. PMHS specific parameters such as age and anthropometry are also variations that are not considered in the current version of the GHBMC FE model which is representative of a 50^{th} percentile male. Adjusting the material properties based on patient-specific biometrics such as bone mineral density should improve correlation between the FE model and the specific experimental results.

Finally, an area which must be addressed in future lower limb models is ankle joint laxity. Since no cartilage exists in the FE model, contact between ankle bones may not be as tightly coupled as in vivo, and the ankle kinematics resulting from an axial load may be affected. Further, the lack of cartilage in the FE model may be responsible for the higher frequency oscillations observed near the peak in the full modified model simulation (Figure 6). While most of the ankle laxity is removed during the preload phase, ankle laxity in the FE model may cause the ankle to prematurely roll and induce a lateral component to the loading on the tibia. This rolling may affect the corresponding tibia strain response. The experimental strain response demonstrates nearly pure axial loading of the tibia, with similar strain amplitudes around the circumference of the tibia shaft. However, the strain response in the FE model suggests some amount of bending may be occurring since the variation of strain amplitude around the circumference of the tibia shaft is large. More experimentation, potentially with the use of a high-speed x-ray system, may be necessary to validate the kinematics of the ankle model and to determine whether the tibia bending phenomenon is accurate or just a result of the ankle roll in the FE model.

V. CONCLUSIONS

This study focused on the development of a constitutive model for human heel pad that could be used in high-rate axial impact applications including UBB. Utility of the constitutive model was evaluated using an FE model of the human lower limb, foot and ankle that was previously developed for automotive intrusion applications. Although this FE model was validated for a multitude of loading conditions typically associated with automotive type loadings, it failed to capture the mechanical response of the lower limb at high-rate, low stroke axial impact. Modifications to the FE model including updated heel properties which incorporated rate sensitivity, mesh refinement and updated bone properties substantially improved biofidelity at the higher loading rates. The modified FE model reproduced the complex internal strain and external force loading characteristics of the PMHS lower limb tests with reasonably good accuracy. This work establishes some of the preliminary efforts required for the development of a more effective and biofidelic modeling tool that may be used to evaluate future systems designed to mitigate injury in blast type loading events.

VI. ACKNOWLEDGEMENT

The authors would like to thank Dr. James Stone for the use of his laboratory equipment for materials testing.

VII. REFERENCES

[1] Vasquez K, Logsdon K, Shivers B, Chancey C. Medical Injury Data, 2011. Unclassified//Public Release.
[2] Ramasamy A, Masouros SD, et al. In-vehicle extremity injuries from improvised explosive devices: current and future foci. *Philosophical Transactions of the Royal Society B: Biological Sciences*, 2011, 366(1562):160-170.
[3] McKay BJ, Bir CA. Lower extremity injury criterion for evaluating military vehicle occupant injury in underbelly blast events. *Stapp Car Crash Journal*, 2009, 53:229-249.
[4] Crandall J, Klopp G, Klisch S, Sieveka S, Pilkey W, Martin P. Research program to investigate lower extremity injuries. *Society of Automotive Engineers*, 1994, Paper 940711.
[5] Yue N, Shin J, Untaroiu C. Development and validation of an occupant lower limb finite element model. *SAE Technical Paper*, 2011, 01, 1128.
[6] Shin J, Yue N, Untaroiu C. A finite element model of the foot and ankle for automotive impact applications. *Annals of Biomedical Engineering*, 2012, 40(12):2519-2531.
[7] Erdemir A, Viveiros ML, Ulbrecht JS, and Cavanagh PR. An inverse finite-element model of heel-pad indentation. *Journal of Biomechanics*, 2006, *39*(7):1279-1286.
[8] Natali AN, Fontanella CG, Carniel EL. Constitutive formulation and analysis of heel pad tissues mechanics. *Medical Engineering & Physics*, 2010, *32*(5):516-522.
[9] Wood GW, Panzer MB, Bass CR, Myers BS. Viscoelastic properties of Hybrid III head skin. *SAE International Journal of Materials & Manufacturing*, 2010, *3*(1):186-193.
[10] Henderson K, Bailey A, Christopher J, Brozoski F, Salzar R. Biomechanical response of the lower leg under high rate loading. *Proceedings of IRCOBI Conference,* 2013, Gothenburg, Sweden.
[11] Fung YC, Biomechanics: Mechanical Properties of Living Tissues, 277-280, *Springer*, New York, NY, 1993.
[12] Ledoux WR, Meaney DF, Hillstrom HJ. A quasi-linear, viscoelastic, structural model of the plantar soft tissue with frequency-sensitive damping properties. *Journal of Biomechanical Engineering*, 2004, 126(6):831-837.
[13] Ledoux WR, and Blevins JJ. The compressive material properties of the plantar soft tissue. *Journal of Biomechanics*, 2007, 40(13):2975-2981.
[14] Carter DR, and Hayes WC. The compressive behavior of bone as a two-phase porous structure. *Journal of Bone and Joint Surgery*, 1977, 59(7):954-962.

[15] Lindahl O. Mechanical properties of dried defatted spongy bone. *Acta Orthopaedica*, 1976, 47(1):11-19.
[16] Morgan EF, and Keaveny TM. Dependence of yield strain of human trabecular bone on anatomic site. *Journal of Biomechanics*, 2001, 34(5):569-577.
[17] Keaveny TM, Morgan EF, Niebur GL, and Yeh OC. Biomechanics of Trabecular Bone. *Annual Reviews in Biomedical Engineering*, 2001, 3(1), 307-333.
[18] Gehre C, Gades H, Wernicke P. Objective rating of signals using test and simulation responses. In *21st International Technical Conference on the Enhanced Safety of Vehicles Conference (ESV)*, 2009, 09-0407.
[19] Gefen A, Megido-Ravid M, Itzchak Y. In vivo biomechanical behavior of the human heel pad during the stance phase of gait. *Journal of Biomechanics*, 2001, 34(12):1661-1665.
[20] Funk JR, Khaewpong N, et al. The axial injury tolerance of the human foot/ankle complex and the effect of Achilles tension. *Journal of Biomechanical Engineering*, 2002, 124(6):750-757.
[21] Miller-Young JE, Duncan NA, Baroud G. Material properties of the human calcaneal fat pad in compression: experiment and theory. *Journal of Biomechanics*, 2002, 35(12):1523-1531.
[22] McElhaney JH. Dynamic response of bone and muscle tissue. *Journal of Applied Physiology*, 1966, 21(4):1231-1236.
[23] Carter D, Hayes W. Bone compressive strength: the influence of density and strain rate. *Science*, 1976, 194(4270):1174-1176.
[24] Jensen N, Kroner K, Hvid I. Distribution of bone strength at the distal tibia and fibula. *Clinical Biomechanics*, 1988, 4(4):226-231.
[25] Sabry F, Ebraheim N, Mehalik J, Rezcallah A. Internal architecture of the calcaneus: implications for calcaneus fractures. *Foot and Ankle International,* 2000, 21(2):114-118.